

Linear combination of unitaries with exponential convergence

P. Brearley^{1,2} and T. L. Howarth³

¹Centre for Quantum Science and Engineering, University of Manchester, UK

²Department of Mechanical and Aerospace Engineering, University of Manchester, UK

³Department of Aeronautical and Automotive Engineering, Loughborough University, UK

ABSTRACT

We present a general method for decomposing non-unitary operators into a linear combination of unitary operators, where the approximation error decays exponentially. The decomposition is based on a smooth periodic extension of the identity map via the Fourier extension method, resulting in a sine series with exponentially decaying coefficients. Rewriting the sine series in terms of complex exponentials, then evaluating it on the Hermitian and anti-Hermitian parts of a non-unitary operator, yields its approximation by a linear combination of unitaries. When implemented in a quantum circuit, the subnormalisation of the resulting block encoding scales with the double logarithm of the inverse error, substantially improving over the polynomial relationship in existing methods. For hardware or applications with a fixed error budget, we discuss a strategy to minimise subnormalisation by exploiting the overcomplete nature of the Fourier extension basis. This regularisation procedure traces an error-subnormalisation Pareto front, identifying coefficients that maximise the subnormalisation at a fixed error budget. Fourier linear combinations of unitaries thus provides an accurate and versatile framework for non-unitary quantum computing.

1. Introduction

Linear combination of unitaries (LCU) is a foundational primitive in quantum computing for constructing unitary block encodings that perform non-unitary maps on a subspace of the overall Hilbert space.¹ Its original development, however, was motivated by simulating unitary quantum dynamics by linear combinations of product formulas,¹ known as multi-product formulas.² It has since become a standard technique for non-unitary quantum computing, being incorporated into algorithms for solving systems of linear equations,³ differential equations,⁴ open quantum systems,⁵ imaginary time evolution,⁶ and fluid dynamics.⁷ It also finds utility in the quantum singular value transformation (QSVT) workflow,⁸ which has emerged as one of the most influential quantum algorithms of the past decade.⁹ By processing the singular values of a non-unitary operator by a prescribed polynomial when presented as a unitary block encoding, it opens up a range of new applications based on matrix arithmetic.¹⁰

The utility of LCU in quantum algorithms depends on the identification of an efficient linear combination of unitary operators that recovers the desired non-unitary operator. Exact constructions for general non-unitary operators require a linear combination of an exponential number of unitaries,¹¹ so exact methods are limited to operators with simple, sparse structures. For example, s -sparse circulant operators can be constructed by a linear combination of s unitaries,¹² which can be extended to general banded operators such as Toeplitz and Hankel using pairs of unitaries that correct the boundary values.¹³ Banded operators are common in several areas of computational science, such as in the numerical simulation of partial differential equations (PDEs) with constant transport coefficients. However, such applications are trivial for classical computers in most contexts. Industries where quantum computing is poised to add the most value are dominated by variable-coefficient PDEs, where material properties or quantities such as the velocity field have spatial dependence. Finding efficient general techniques for approximating non-unitary operators by LCU provides a route for simulating industrially relevant problems on quantum computers, as well as providing a robust access point for QSVT.⁹

The prevailing general decomposition in the literature is the following linear combination of four unitaries,⁵

$$A = \frac{ie^{-i\tau H_1} - ie^{i\tau H_1} + e^{i\tau H_2} - e^{-i\tau H_2}}{2\tau} + O(\tau^2), \quad (1)$$

where

$$H_1 = \frac{A + A^\dagger}{2}, \quad H_2 = \frac{A - A^\dagger}{2i} \quad (2)$$

are Hermitian operators such that $A = H_1 + iH_2$.¹⁴ This method was used by Schlimgen et al.⁵ for simulating Markovian open quantum dynamics, and later applied in various other contexts.^{15,16} The decomposition approximates the Taylor expansion of the sine function

$$\frac{\sin(\tau\theta)}{\tau} = \frac{e^{i\tau\theta} - e^{-i\tau\theta}}{2\tau i} = \theta + O(\tau^2\theta^3). \quad (3)$$

It becomes a linear combination of two unitaries when applied to Hermitian matrix inputs $H = H^\dagger$,

$$H = \frac{e^{i\tau H} - e^{-i\tau H}}{2\tau i} + O(\tau^2), \quad (4)$$

which is accurate to order 2. Anti-Hermitian matrices iH can equivalently be expressed as a linear combination of unitaries by multiplying Eq. (4) by i . Since all non-unitary matrices can be separated into their Hermitian and anti-Hermitian components $A = H_1 + iH_2$ by Eq. (2), then any non-unitary operator can be approximated by a linear combination of at most four unitary operators by summing the decompositions for H_1 and iH_2 to yield Eq. (1). When implemented in a quantum circuit,¹ this prepares a unitary block encoding of A/α to error ϵ , where α is the subnormalisation. The disadvantage of the decomposition in Eq. (1) is that by reducing τ to reduce the error by $\epsilon = O(\tau^2)$, the subnormalisation is increased by $\alpha = O(1/\tau)$, which penalises the probability of successful postselection by $O(\tau^2)$. Therefore, finding alternatives to Eq. (1) where the ϵ decay outpaces the increase in α will greatly increase the applicability of general LCU decompositions, and retrospectively improve the algorithms based on Eq. (1).^{5,15,16}

Conceptually, Eq. (4) is differentiating $e^{i\tau H}$ with respect to τ , since the result is proportional to iH at small τ . Therefore, the order may be arbitrarily improved upon by higher-order finite difference methods. The approximation to even order p is

$$A = \sum_{k=1}^{p/2} b_k \frac{ie^{-ik\tau H_1} - ie^{ik\tau H_1} + e^{ik\tau H_2} - e^{-ik\tau H_2}}{\tau} + O(\tau^p). \quad (5)$$

where b_k are the central finite difference coefficients for a constant grid spacing, e.g. $b_1 = 1/2$ for $p = 2$ and $b_1, b_2 = 2/3, -1/12$ for $p = 4$. This simple extension is already a significant improvement, since $\epsilon = O(\tau^p)$ while the subnormalisation becomes $\alpha = O([1/\tau] \log p)$. Such approximations to order p are yet to be utilised for quantum algorithm development, to the best of our knowledge. Despite the improved scaling, the $\alpha = \text{poly}(1/\epsilon)$ relationship remains. This requires the extensive use of amplification techniques^{9,17} for applications requiring a reasonable accuracy or repeated applications of the non-unitary operator,¹⁸ which becomes expensive and impractical at large α as the signal is lost to noise. In this work, we derive a general LCU decomposition that converges exponentially in the number of unitaries $m = O(\log 1/\epsilon)$, where the subnormalisation $\alpha = O(\log \log 1/\epsilon)$, dramatically improving on the decomposition in Eq. (5).

The LCU decomposition is based on the Fourier extension method, and is presented in Section 2. For readers looking for a ‘quick start’, the decomposition itself can be found in Eq. (9), and the corresponding coefficients in Table A of the appendix. Section 3 presents the quantum circuit implementation and derivation of the LCU subnormalisation α . The method of computing the Fourier extension coefficients is discussed in Section 4, including the exponentially converging coefficients in 4.1 (Table A) and subnormalisation-optimal coefficients in 4.2 (Table B). Section 5 justifies the algorithmic complexity of the Fourier-LCU approach. The theoretical results are supported by numerical examples in Section 6, using statevector simulations of the density matrix for a simple Markovian open quantum system. Finally, we discuss conclusions and outlook in Section 7.

2. Fourier-LCU Decomposition

The function $f(\tau) = \tau$ is approximated on the subinterval $[-\pi/\eta, \pi/\eta]$ of a periodic domain $[-\pi, \pi]$ by the Fourier extension method, where η is the domain extension factor. Since $f(\tau)$ is odd, it can be expressed as the sine series

$$f(\tau) \approx \sum_{k=1}^m a_k \sin(k\tau). \quad (6)$$

A sawtooth wave is obtained for $\eta = 1$, where the $[-\pi, \pi]$ domain repeats without a buffer zone, causing a discontinuity in $f(\tau)$. This may be approximated with the analytical coefficients $a_k = (2/k)(-1)^{k-1}$. However, these decay as $1/k$ due to the jump discontinuity, thereby not improving upon the finite difference approximation in Eq. (3). For exponential convergence, the function must be smooth and periodic on $[-\pi, \pi]$, which can be achieved by taking $\eta > 1$ and identifying the corresponding coefficients a_k such that the 2π -periodic series approximates $f(\tau)$ on the interior subinterval $[-\pi/\eta, \pi/\eta]$.

The Fourier extension sine series in Eq. (6) can be applied to matrix inputs τH when its eigenvalues are within the evaluated interval, allowing H to be approximated to exponential accuracy by

$$H \approx \frac{1}{\tau} \sum_{k=1}^m a_k \sin(k\tau H), \quad \text{spec}(\tau H) \subseteq [-\pi/\eta, \pi/\eta]. \quad (7)$$

Hence, τ should be chosen such that $\tau \|H\|_2 \leq \pi/\eta$, so $\tau = \pi/(\eta \|H\|_2)$ is the optimal choice. The identity

$$\sin(k\tau H) = \frac{e^{ik\tau H} - e^{-ik\tau H}}{2i}, \quad (8)$$

is a linear combination of unitary operators when $H = H^\dagger$, and can be substituted into Eq. (7) to express H as a linear combination of unitary operators with exponential convergence. Since a general non-unitary operator $A = H_1 + iH_2$ can be separated into a Hermitian component H_1 and an anti-Hermitian component iH_2 by Eq. (2), then any non-unitary operator can be expressed as the linear combination of the following $4m$ unitary operators

$$A \approx \sum_{k=1}^m \frac{a_k}{2\tau} \left(ie^{-ik\tau H_1} - e^{-ik\tau H_2} - ie^{ik\tau H_1} + e^{ik\tau H_2} \right), \quad (9)$$

with exponential convergence in m . Here, $\tau = \pi/(\eta \max[\|H_1\|_2, \|H_2\|_2])$ is chosen to ensure that the spectra of both H_1 and H_2 lie within $[-\pi/\eta, \pi/\eta]$. Coefficients for the decomposition are provided in Table A using $\eta = 2 + 0.460m^{-0.319}$, which we show minimises αm in Section 4. Unlike in the decompositions based on the finite difference method in Eq. (5), the parameter τ is $O(1)$, and additional accuracy is provided solely by increasing m .

3. Quantum Circuit Implementation

Equation (9) provides a means of expressing a non-unitary operator $A \approx \sum_{j=1}^{4m} \kappa_j U_j$ as a sum of $4m$ unitary operators U_i with weights κ_j , where the error of the approximation decays exponentially in m . It can be implemented by LCU using the quantum circuit shown in Fig. 1. The weights κ_j are defined as

$$\kappa_j = \frac{a_{\lceil j/4 \rceil}}{2\tau} e^{i\frac{\pi}{2}j}, \quad j = 1, 2, \dots, 4m, \quad (10)$$

where $e^{i\frac{\pi}{2}j}$ supplies the unitaries' global phase $(i, -1, -i, 1)$ in Eq. (9). The square roots of the magnitude of the $4m$ coefficients are encoded into the first column of a unitary V as

$$V_{i,0} = \sqrt{\frac{|\kappa_i|}{\sum_{j=1}^{4m} |\kappa_j|}}. \quad (11)$$

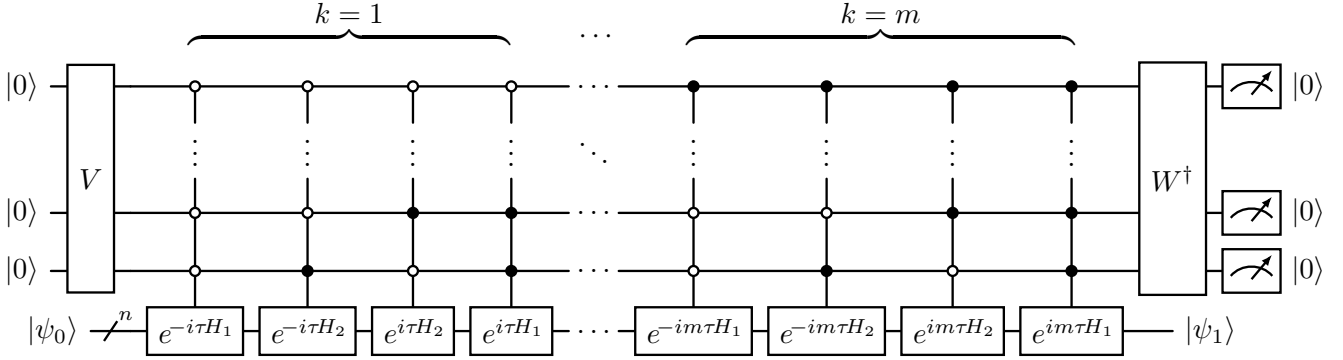


Figure 1. Quantum circuit for Fourier LCU, implementing the decomposition in Eq. (9). The unitaries V and W are defined in Eqs. (11) and (12) respectively.

Then, the phases are encoded into the first column of a second unitary, W , defined as

$$W_{i,0} = \frac{\kappa_i^*}{|\kappa_i|} \sqrt{\frac{|\kappa_i|}{\sum_{j=1}^{4m} |\kappa_j|}}, \quad (12)$$

such that $V_{i,0}W_{i,0}^* = \kappa_i/\alpha$, with $\alpha = \sum_{j=1}^{4m} |\kappa_j|$ and the asterisk denoting the complex conjugate. When m is a power of 2, the $4m$ coefficients occupy the entire first columns of V and W , which act on $n_a = \lceil \log_2(4m) \rceil$ ancilla qubits. The remaining columns are chosen to form an orthonormal basis, which ensures that V and W are both unitary.

The LCU algorithm proceeds as follows.¹ The unitary V is applied to n_a ancilla qubits initialised in the state $|0\rangle^{\otimes n_a}$, such as to prepare the amplitudes by the first column of V , with the remaining arbitrary orthonormal columns having no effect. Then, the unitary operators U_i are applied to the main register with a control configuration on the ancilla register to isolate the corresponding coefficient. Finally, W^\dagger is applied to combine the remaining magnitude and phase information, finalising the map

$$|0\rangle^{\otimes n_a} |\psi\rangle \mapsto |0\rangle^{\otimes n_a} \frac{\sum_{j=1}^{4m} \kappa_j U_j}{\sum_{j=1}^{4m} |\kappa_j|} |\psi\rangle + \dots, \quad (13)$$

as derived by Childs & Wiebe.¹ This is a $(\alpha, n_a, \varepsilon)$ -block encoding of A as given in Definition 1. Measuring the ancilla qubits to be $|0\rangle^{\otimes n_a}$ therefore prepares a state $A/\alpha |\psi\rangle$ up to error ε .

Definition 1 (Block encoding). *Suppose that A is an n -qubit operator, $\alpha, \varepsilon \in \mathbb{R}_+$, and $n_a \in \mathbb{N}$. We say that the $(n + n_a)$ -qubit unitary U is an $(\alpha, n_a, \varepsilon)$ -block-encoding of A if $\|A - \alpha(|0\rangle^{\otimes n_a} \otimes I)U(|0\rangle^{\otimes n_a} \otimes I)\|_2 \leq \varepsilon$.*

The LCU subnormalisation in Eq. (13) is $\alpha = \sum_{j=1}^{4m} |\kappa_j|$, which expands to

$$\alpha = \frac{2}{\pi} \sum_{k=1}^m |a_k| = \frac{2\eta}{\pi} \max[\|H_1\|_2, \|H_2\|_2] \sum_{k=1}^m |a_k| \quad (14)$$

for Fourier LCU by the decomposition in Eq. (9). Hence, α depends on the choice of η , the operator scale $\max[\|H_1\|_2, \|H_2\|_2]$, and the coefficient L^1 -norm $\sum_{k=1}^m |a_k|$. The dependence on these parameters will be derived in the complexity analysis in Section 5.

4. Coefficient Selection Strategy

4.1 Exponential convergence via least squares

For $\tau \in [-\pi/\eta, \pi/\eta]$, the coefficients $\mathbf{a}^{\text{LS}} = [a_1^{\text{LS}}, a_2^{\text{LS}}, \dots, a_m^{\text{LS}}]^\top$ are the solution to the continuous least-squares problem

$$\mathbf{a}^{\text{LS}} \in \arg \min_{\tilde{a} \in \mathbb{R}^m} \int_{-\pi/\eta}^{\pi/\eta} \left(\tau - \sum_{k=1}^m \tilde{a}_k \sin(k\tau) \right)^2 d\tau, \quad (15)$$

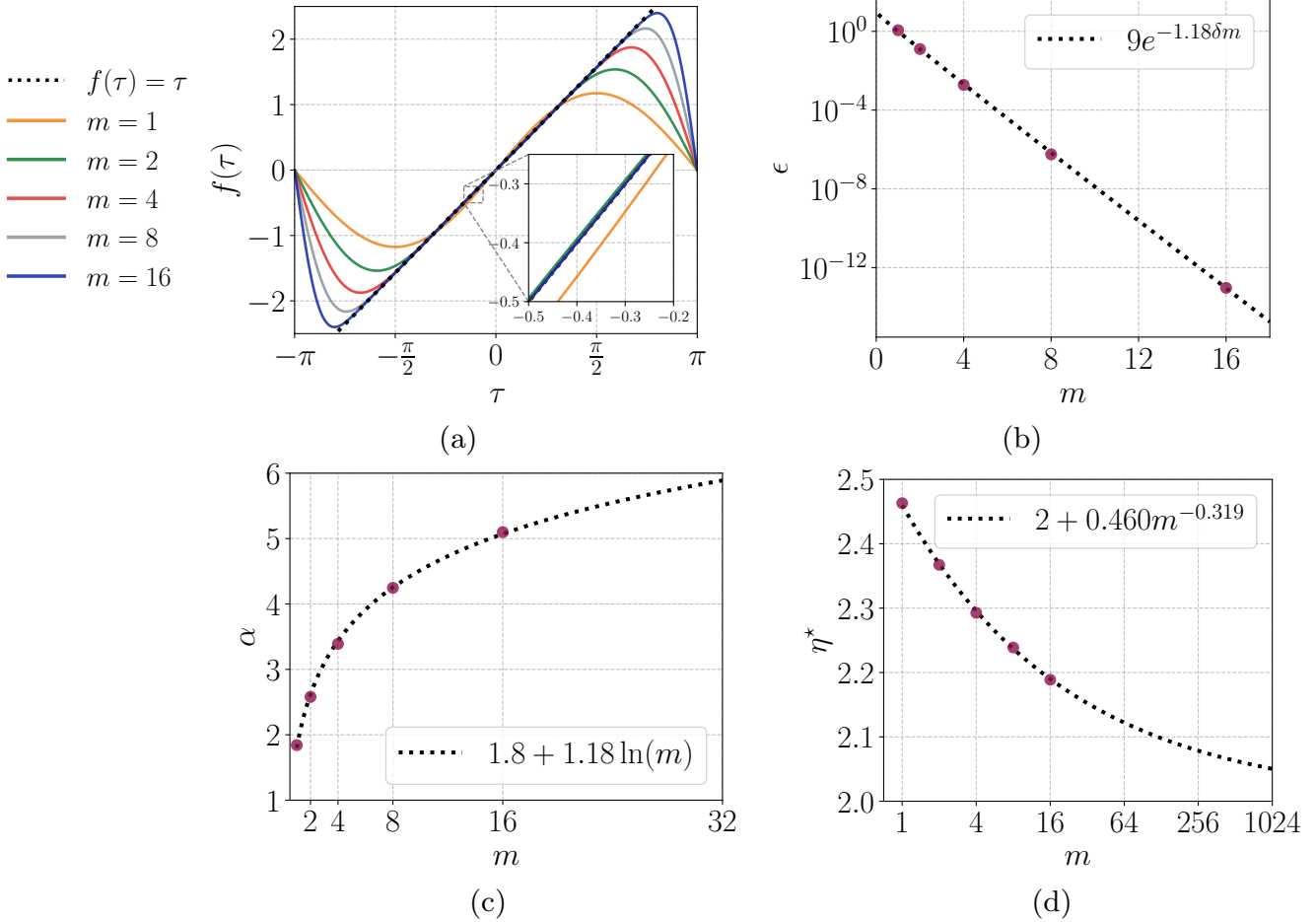


Figure 2. (a) Fourier extension sine series to approximate $f(\tau) = \tau$ by Eq. (6) on the subinterval $\tau \in [-\pi/\eta, \pi/\eta]$, corresponding to $\eta = 2 + 0.460m^{-0.319}$, using the coefficients given in Table A. (b) Error L^2 norm on $[-\pi/\eta, \pi/\eta]$. (c) Block-encoding subnormalisation given by Eq. (14). (d) Optimal extension factor η to minimise $m\alpha$ given by Eq. (18).

which we evaluate using Gauss-Legendre quadrature. The coefficients for various m are shown in Table A, using $\eta = 2 + 0.460m^{-0.319}$, which will be derived shortly. The sine series for up to $m = 16$ terms is plotted in Fig. 2a, with the L^2 error, subnormalisation α , and extension factor η shown in Figs. 2b, 2c and 2d respectively. Figure 2 demonstrates the exponential convergence in the Fourier extension, with the $m = 16$ case approaching the double-precision floating-point accuracy common in classical simulators. Furthermore, the LCU normalisation in Fig. 2c reveals that such high accuracy can be achieved without excessive subnormalisation, $\alpha \approx 5$.

We now derive the choice of the extension parameters $\eta = 2 + 0.460m^{-0.319}$ used for the presented coefficients in Table A. Increasing η in the Fourier extension fits $f(\tau) = \tau$ on a smaller interval $[-\pi/\eta, \pi/\eta]$. Over the η and m range relevant to this study, we observe that the error decays exponentially with the thickness of the buffer zone $\delta(\eta) = \pi - \pi/\eta$, although note that this is not always the case.¹⁹ Therefore, with the assumption of $\varepsilon = O(e^{-\delta(\eta)m})$, η must be chosen such that $\delta(\eta)$ is sufficiently large that the rate of exponential convergence in m is not prohibitive. We choose η to minimise the LCU cost quantified by $m\alpha$, since LCU circuit depth scales linearly in m ,¹ and the amplitude amplification cost scales linearly in α .^{17,20} Defining $S_m(\eta) = \sum_{k=1}^m |a_k(\eta)|$ and assuming $\max[\|H_1\|_2, \|H_2\|_2] = 1$ as is common for evolution operators, then $\alpha(m, \eta) = (2\eta/\pi)S_m(\eta)$. The required number of terms scales as

$$m = O\left(\frac{1}{\delta(\eta)} \log \frac{1}{\varepsilon}\right) \quad (16)$$

such that the LCU cost is

$$m\alpha = O\left(\frac{\eta S_m(\eta)}{\delta(\eta)} \log \frac{1}{\varepsilon}\right). \quad (17)$$

Since ε is not a direct function of η , minimising the LCU cost amounts to minimising $\eta S_m(\eta)/\delta(\eta)$. If $S_m(\eta)$ is differentiable, then a minimum can be found at η^* corresponding to

$$\eta^* \frac{S'_m(\eta^*)}{S_m(\eta^*)} = \frac{2 - \eta^*}{\eta^* - 1}. \quad (18)$$

Therefore, evaluating η^* relies on the accurate evaluation of

$$S'_m(\eta) = \sum_{k=1}^m \text{sgn}(a_k(\eta)) a'_k(\eta), \quad (19)$$

where $a'_k(\eta)$ is obtained by implicitly differentiating the least-squares optimality condition $G(\eta)a(\eta) = b(\eta)$ with respect to η , and solving the resulting linear system. The obtained η^* values are plotted in Fig. 2d, with the fitted function $\eta = 2 + 0.460m^{-0.319}$. This suggests that $\eta^* \rightarrow 2$ as $m \rightarrow \infty$, implying that $S'_\infty(2) = 0$.

4.2 Optimal subnormalisation via regularised fitting

While the number of basis functions m grows logarithmically with the desired accuracy, the LCU subnormalisation α also grows with m when coefficients are optimised solely for least-squares error, and we derive the exact dependence in the following section. By regularising the objective function, we exploit the overcomplete nature of the Fourier extension basis to identify coefficient vectors that significantly reduce α without sacrificing fidelity, in a manner analogous to basis pursuit from classical signal processing.²¹

In a standard Fourier series ($\eta = 1$), the dictionary $\Phi = \{\sin(k\tau)\}_{k=1}^m$ forms an orthonormal basis, yielding a unique mapping from functions to coefficients. In our framework ($\eta > 1$), the Fourier basis is defined over an extended domain larger than the physical interval. When restricted to the physical domain, the dictionary becomes overcomplete; the basis functions are no longer linearly independent, producing a non-trivial null space and a continuum of coefficient vectors representing the same function with identical L_2 error. We define the regularised loss function as

$$J(\mathbf{a}; \lambda, \eta) = \underbrace{\|\tau - \Phi \mathbf{a}\|_2}_\varepsilon + \lambda \underbrace{\frac{2\eta}{\pi} \|\mathbf{a}\|_1}_\alpha, \quad (20)$$

where $\Phi \mathbf{a} = \sum_{k=1}^m a_k \sin(k\tau)$ denotes the reconstruction of the function from the coefficient vector $\mathbf{a} \in \mathbb{R}^m$, and λ is a tunable hyperparameter controlling the trade-off between error and subnormalisation. Before presenting numerical results, we first state and prove a series of useful properties of this optimisation problem.

Lemma 1 (Monotonicity of the joint functional J). *Let $J_m^*(\lambda; \eta)$ be the minimum value of the cost function J for a dictionary of size m , and let \mathbf{a}_m^* be the corresponding optimal coefficient vector. For a fixed regularisation parameter $\lambda > 0$ and extension parameter $\eta > 1$, the sequence of optimal costs $\{J_m^*\}_{m=1}^\infty$ is monotonically non-increasing.*

Proof. Consider the nested subspaces of the Fourier extension $V_m = \text{span}\{\sin(k\tau)\}_{k=1}^m$, where $V_m \subset V_{m+1}$. Let $\mathbf{a}_m^* = [a_1, \dots, a_m]^\top$ be the optimal solution for a basis of size m . We construct a candidate solution $\tilde{\mathbf{a}}_{m+1}$ for the basis of size $m+1$ by padding \mathbf{a}_m^* with a zero:

$$\tilde{\mathbf{a}}_{m+1} = \begin{bmatrix} \mathbf{a}_m^* \\ 0 \end{bmatrix}.$$

Since $\tilde{\mathbf{a}}_{m+1} \in \mathbb{R}^{m+1}$, it exists in the search space of the $(m+1)$ -order optimisation problem. The loss associated with this candidate is:

$$J_{m+1}(\tilde{\mathbf{a}}_{m+1}; \lambda, \eta) = \|\tau - \Phi_{m+1} \tilde{\mathbf{a}}_{m+1}\|_2 + \lambda \frac{2\eta}{\pi} \|\tilde{\mathbf{a}}_{m+1}\|_1.$$

Because the $(m+1)$ -th column of Φ_{m+1} is multiplied by zero, the reconstruction $\Phi_{m+1}\tilde{\mathbf{a}}_{m+1}$ reduces exactly to $\Phi_m \mathbf{a}_m^*$. Furthermore, $\|\tilde{\mathbf{a}}_{m+1}\|_1 = \|\mathbf{a}_m^*\|_1$. Thus:

$$J_{m+1}(\tilde{\mathbf{a}}_{m+1}; \lambda, \eta) = \|\tau - \Phi_m \mathbf{a}_m^*\|_2 + \lambda \frac{2\eta}{\pi} \|\mathbf{a}_m^*\|_1 = J_m^*(\lambda; \eta).$$

The optimal solution \mathbf{a}_{m+1}^* is the minimiser over the entire space \mathbb{R}^{m+1} ; hence, by definition:

$$J_{m+1}^* \leq J_{m+1}(\tilde{\mathbf{a}}_{m+1}; \lambda, \eta) = J_m^*.$$

□

While the monotonicity of J holds for any basis, the transition into an overcomplete regime enables a specific redundancy arbitrage. Because the dictionary possesses a non-trivial null space, the optimiser can navigate a manifold of equivalent solutions, all yielding the same approximation error ε , to identify the one that minimises the subnormalisation α . In a standard orthonormal basis, this manifold collapses to a single point, offering no choice in coefficient distribution; in our overcomplete dictionary, it provides the freedom to significantly reduce the subnormalisation cost without sacrificing fidelity.

Corollary 1.1 (Monotonicity of α^* for a fixed error budget). *Let $\alpha_m^*(\varepsilon; \eta)$ be the minimum LCU subnormalisation required to achieve a target error $\|\tau - \Phi_m \mathbf{a}\|_2 \leq \varepsilon$ using a basis of size m . Then the sequence $\{\alpha_m^*\}_{m=1}^\infty$ is monotonically non-increasing.*

Proof. Let $F_m(\varepsilon) = \{\mathbf{a} \in \mathbb{R}^m : \|\tau - \Phi_m \mathbf{a}\|_2 \leq \varepsilon\}$ be the feasible set of coefficients. Since $\Phi_{m+1}[\mathbf{a}, 0]^\top = \Phi_m \mathbf{a}$, any solution in $F_m(\varepsilon)$ has a corresponding representation in $F_{m+1}(\varepsilon)$ with an identical L_1 -norm. Thus, $F_m \subseteq F_{m+1}$. Minimising the L_1 -norm over a strictly expanding feasible set ensures that the optimal value α_m^* cannot increase. □

Corollary 1.2 (Existence of α_∞^*). *For a fixed ε and η , the sequence $\{\alpha_m^*\}_{m=1}^\infty$ converges to a finite limit α_∞^* as $m \rightarrow \infty$.*

Proof. By Corollary 1.1, the sequence $\{\alpha_m^*\}_{m=1}^\infty$ is monotonically non-increasing. Since α is non-negative, the sequence is bounded below. Therefore, by the monotone convergence theorem for real sequences, it converges to a finite limit. □

These theoretical results suggest that the optimiser can exploit the null space to reduce α . We now demonstrate this numerically. In the following examples, we use the same extension parameter (η^*) identified in Section 4.1. To identify the most efficient solution in practice, we sweep the hyperparameter λ , warm-starting each iteration from the previous solution. This procedure traces out a Pareto front: a boundary representing the optimal trade-off between ε and α . Any point on this curve is Pareto-optimal; the error cannot be reduced without increasing the subnormalisation cost.

As shown in the right-hand panel of Figure 3, these fronts eventually flatline, numerically validating the existence of the stable cost limit α_∞^* . We compare these optimal fronts against the baseline of standard unregularised optimisation. The horizontal lines in Figure 3 indicate the values α_m^{LS} obtained via standard least-squares fits in Section 4.1. The vertical gap between these lines and our regularised curves represents the subnormalisation that is recovered by our method. In this case, α for $m = 32$ and $m = 64$ is smaller than for $m = 2$, despite providing significantly higher accuracy. Table B provides these coefficients for $m = 8, 16, 32, 64$ for $\lambda \rightarrow 0$.

Interestingly, for small basis sizes ($m \leq 6$ for $\eta = 2$), the regularised solutions are identical to the least-squares results. In this low-resolution regime, the basis functions are sufficiently distinct that no appreciable null space exists to be exploited. As m increases, the dictionary Φ becomes increasingly overcomplete, and the solutions begin to diverge. This transition point depends on the extension parameter η ; a larger η results in higher basis redundancy at lower frequencies, allowing for a quicker transition to the regime where the subnormalisation cost can be optimised.

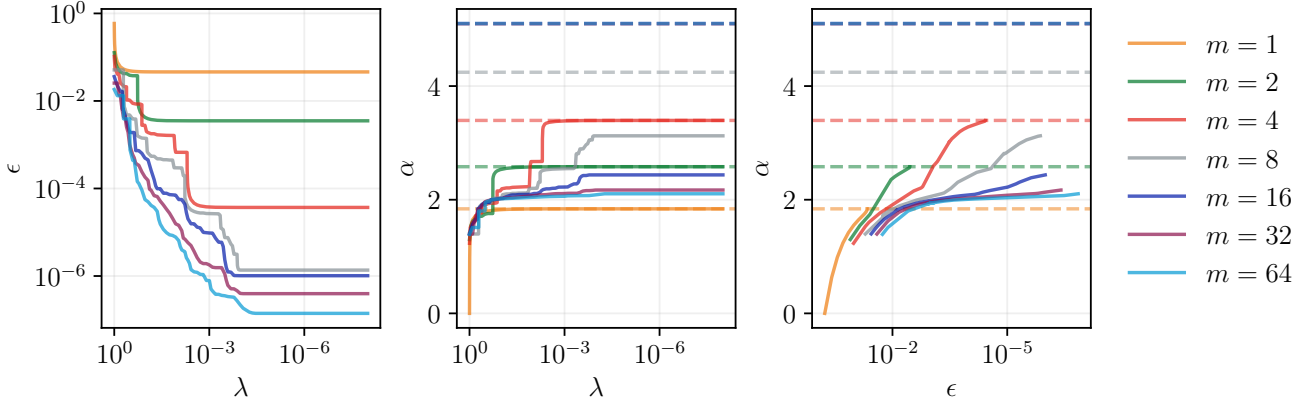


Figure 3. Left and centre: The relationship between λ , ϵ , and α . As $\lambda \rightarrow 0$, the solver trades subnormalisation for higher precision. Right: The Pareto front. The horizontal lines show the cost of standard least-squares fits \mathbf{a}^{LS} . The vertical distance to the regularised curves represents the subnormalisation improvement, with the flatlining behaviour demonstrating convergence to the stable limit α_∞^* .

While the λ -sweep characterises the entire trade-off landscape, a practitioner typically operates with a specific error budget ϵ_{target} dictated by the specific application and the hardware's noise floor. In this case, a root-finding procedure such as Brent's method²² can be used to find the largest λ that satisfies the constraint

$$\|\tau - \Phi \mathbf{a}\|_2 = \epsilon_{\text{target}} \quad (21)$$

on the Pareto curve in Figure 3.

5. Resource Requirements

The presented Fourier LCU prepares an (α, n_a, ϵ) -block encoding of A using a linear combination of $O(m)$ Hamiltonian simulations. The number of controlling qubits per Hamiltonian simulation scales as $n_a = O(\log m)$, and since an n_a -controlled Toffoli gate can be decomposed into $O(n_a)$ CNOT gates,²³ the quantum circuit in Fig. 1 can be expressed as $O(m)$ Hamiltonian simulations each surrounded by $O(\log m)$ CNOT gates. Optimal Hamiltonian simulation of $e^{\pm ik\tau H}$ in Eq. (9) requires $O(s\|H\|_{\max} k\tau + \log[1/\epsilon])$, gates assuming oracular access to the Hamiltonian,²⁴ where $k = O(m)$, s is the sparsity and $\|H\|_{\max}$ is the largest absolute entry of H . If $A = H_1 + iH_2$ is s -sparse, then H_1 and H_2 are $O(s)$ -sparse. We assume that both $\|H_1\|_{\max}$ and $\|H_2\|_{\max}$ are $O(\|A\|_2)$. Since $\tau = \pi/(\eta \max[\|H_1\|_2, \|H_2\|_2])$ and $\eta = 2 + 0.460m^{-0.319} = O(1)$, then $\tau = O(1/\|A\|_2)$. Combining these contributions, preparing a single (α, n_a, ϵ) -block encoding of A requires $O([sm + \log\{1/\epsilon\}]m \log m)$ gates. Using $m = O(\log[1/\epsilon])$, this becomes $O([s + 1]\log^2[1/\epsilon] \log \log[1/\epsilon])$ gates.

If the ancilla qubits are immediately measured, they are found in the $|0\rangle^{\otimes n_a}$ state with a probability $1/(\alpha Q)^2$, where $Q = \|\vec{\psi}_0\|_2/\|\vec{\psi}_1\|_2$ for unnormalised solution vectors $\vec{\psi}_1 = A\vec{\psi}_0$. Therefore, this requires $O(\alpha^2 Q^2)$ attempts per successful run. With prior knowledge of the input state $|\psi_0\rangle$, α and Q , then amplitude amplification improves the probability to $O(1)$ using $O(Q\alpha)$ applications of the (α, n_a, ϵ) -block encoding of A .¹⁷ Therefore, the overall gate complexity of a single application of Fourier LCU is $O(Q\alpha[s + 1]\log^2[1/\epsilon] \log \log[1/\epsilon])$ gates. The expression will now be further refined by deriving the scaling of α .

Equation (14) shows that α depends on linearly on η , $\max(\|H_1\|_2, \|H_2\|_2)$, and S_m , where we have already justified that $\eta = O(1)$ and $\max(\|H_1\|_2, \|H_2\|_2) = O(\|A\|_2)$. Considering the behaviour of the final term S_m , we observe that $|a_k|$ decays exponentially in k with up to $m = 16$ terms, beyond which classical double-precision floating-point accuracy is reached. This convergence ordinarily implies that $\sum_{k=1}^m |a_k|$ converges to a finite limit. However, Fourier extensions are known to converge rapidly on the target interval, without necessarily approaching a fixed periodic analytic function.²⁵ Outside of the fitted interval, this can become unbounded and ultimately lead to large, non-decaying Fourier coefficients.²⁵ Therefore, we are unable to conclude that α becomes independent of m .

Instead, we consider the empirical observation $\sum_{k=1}^m |a_k| = O(\log m)$ for the range of $m \leq 16$ relevant to this study, as supported by Fig. 2.

Combining the above contributions, $\alpha = O(\|A\|_2 \log m) = O(\|A\|_2 \log \log(1/\varepsilon))$. This is near-optimal, since α must always scale with $\|A\|_2$ such that it can be block-encoded in a unitary operator U , which enforces $\|U\|_2 = 1$. Therefore, the final gate complexity of Fourier LCU is $O(Q[s+1]\|A\|_2 \log^2[1/\varepsilon] \log^2 \log[1/\varepsilon])$, assuming oracular access to the Hamiltonian. If we invoke the assumption $\|A\|_2 = O(1)$ as typical for contractive evolution operators, this becomes simply $O(Q[s+1] \log^2[1/\varepsilon] \log^2 \log[1/\varepsilon])$ gates. Suppressing the poly-logarithmic error terms, this is simply $\tilde{O}(Qs)$ gates.

In cases where repeated applications of A are required, such as time marching, amplitude amplification in its original form¹⁷ is not possible, since the intermediate states are generally unknown. Oblivious amplitude amplification avoids the need for explicit reflections about an unknown state,²⁶ but requires the target transformation to be approximately unitary. This is because it is unable to distinguish between subnormalisation and the action of the non-unitary operator itself, thereby distorting non-unitary maps.²⁷ QSVD, which generalises quantum signal processing,²⁸ transforms the singular values of a block-encoded non-unitary operator by a prescribed polynomial. Since QSVD acts at the operator level, it transforms the block encoding without distorting the state on which it acts, thus providing a route to amplify block encodings of non-unitary operators obliviously to the quantum state. This is termed uniform singular value amplification, and its potential was demonstrated by Fang, Lin and Tong¹⁸ for algorithms requiring multiple applications of the unitary block encoding, such as time marching for solving differential equations. A single block encoding of $A_T A_{T-1} \cdots A_1$ is prepared that acts on the known input state $|\psi_0\rangle$, such that amplitude amplification¹⁷ can subsequently be applied to obtain an $O(1)$ success probability.¹⁸

6. Numerical Examples

To demonstrate the method numerically, we consider the Markovian open-system dynamics governed by the Lindblad master equation

$$\frac{d\rho}{dt} = -i[H, \rho] + \sum_k \left(L_k \rho L_k^\dagger - \frac{1}{2} \{ L_k^\dagger L_k, \rho \} \right). \quad (22)$$

where ρ is the density matrix, H is the Hamiltonian governing the closed quantum evolution, and L_k are the Lindblad operators modelling the open interactions with the environment. For numerical implementation in a statevector simulation, we consider a vectorised representation of Eq. (22) that is encoded into the amplitudes of a quantum state such that the Lindblad master equation becomes $d|\rho\rangle/dt = M|\rho\rangle$, where M is the Liouvillian superoperator and $|\rho(t)\rangle = A|\rho(0)\rangle$ where $A = e^{Mt}$.

As a minimal example, we consider a single driven qubit subject to pure dephasing. We define the Hamiltonian

$$H = \frac{\omega}{2} (\sigma_x \sin \phi + \sigma_y \cos \phi), \quad (23)$$

where $\sigma_x = |0\rangle\langle 1| + |1\rangle\langle 0|$ and $\sigma_y = -i|0\rangle\langle 1| + i|1\rangle\langle 0|$ are the Pauli operators, ω is the Rabi angular frequency and ϕ is the phase that sets the drive axis in the xy plane. Pure dephasing is modelled by

$$L_\phi = \sqrt{\frac{1}{2T_\phi}} \sigma_z, \quad (24)$$

where T_ϕ is the phase coherence time scale. We choose parameters reflective of an ion-trap qubit rotation with Rabi frequency $\Omega = 10^5$ Hz such that $\omega = 2\pi\Omega$, $\phi = \pi/4$ and $T_\phi = 1$ s,²⁹ evolved for $t = 500/\Omega$ corresponding to 500 Rabi cycles. We initialise the system in the state $\rho(0) = |+\rangle\langle +|$, then vectorise the density matrix and encode the amplitudes in a two-qubit quantum state, i.e. $|\rho(0)\rangle = |+\rangle \otimes |+\rangle$. The deviation of the target propagator from unitarity is quantified by the unitarity defect $\delta_U = \|A^\dagger A - I\|_2 \approx 10^{-2}$. The error between the statevector simulation and the exact evolution is shown in Fig. 4a, the corresponding LCU subnormalisation α in Fig. 4b, and the LCU cost quantified by αm in Fig. 4c

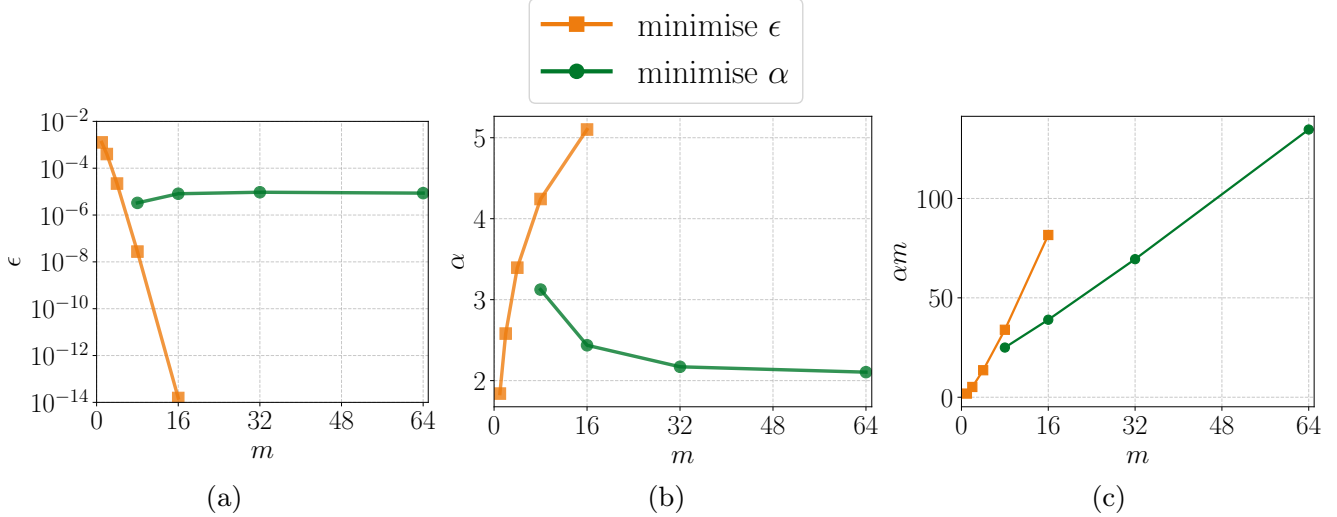


Figure 4. Comparison of the coefficient selection strategies in Section 4 using statevector simulations. (a) Error L^2 norm $\|\langle \rho(t) \rangle - \vec{\rho}(t) \|_2$ between the computed statevector $|\rho(t)\rangle$ and the analytical solution $\vec{\rho}(t)$ rescaled to norm 1, against the number of terms in the Fourier series m , where the number of unitaries in the LCU is $4m$. (b) The subnormalisation α of the resulting block encoding, consistent with the definition in Eq. (14). (c) LCU cost quantified by αm .

Figure 4a demonstrates the exponential convergence in the m terms of the Fourier continuation and in the $4m$ unitaries of the Fourier LCU. The statevector errors closely follow the Fourier continuation errors in Fig. 2, scaled by approximately δ_U . This is consistent with Fourier LCU being exact when A is unitary, so the error for non-unitary A is governed by both the departure from unitary dynamics δ_U and m . Figure 4a shows that for the regularised coefficients derived in Section 4.2, the error of the optimal solution at $\lambda \rightarrow 0$ converges to approximately $\epsilon \approx 10^{-5}$, and hence becomes independent of m . This error tolerance will be sufficient for most applications.

Figure 4b contrasts the α behaviour of both coefficient selection strategies. The least-squares method results in exponential convergence, but without regard for the resulting subnormalisation, which grows as $\alpha = O(\log m)$. Using the regularised coefficients, the relationship is reversed, with α reducing in m as it takes advantage of the increasing redundancy in the Fourier extension. For amplitude amplification to be feasible, the block-encoded operator must maintain a reasonable magnitude so it can be distinguished from noise. For the coefficients optimised for exponential convergence, the most accurate block encoding retains a reasonable signal strength corresponding to a subnormalisation $\alpha \approx 5$, but this improves to $\alpha \approx 2$ for the regularised coefficients. The potential advantage of the regularisation approach is analysed in Fig. 4c, which compares the LCU cost αm between the approaches. This shows that, if the error $\epsilon \approx 10^{-5}$ is sufficient for the chosen application, then $m = 16$ regularised terms can be implemented with comparable resources to $m = 8$ least-squares terms, while reducing the reliance on amplitude amplification by a factor of 1.74. However, this benefit quickly diminishes as α converges, making $m = 64$ terms both less efficient and less accurate than $m = 16$ least-squares terms. Therefore, while the least-squares coefficients are algorithmically superior, the regularised coefficients are useful for constructing high-quality block encodings for practical quantum computation.

7. Conclusions

We have presented a general LCU decomposition that enables non-unitary operators to be block-encoded with an exponentially decaying error, while the corresponding sub-normalisation grows only doubly logarithmically with the inverse error. The main idea is to replace the local Taylor approximations in existing general decompositions with a Fourier extension of $f(\tau) = \tau$. Expressing the sine functions in terms of complex exponentials results in a linear combination of unitaries when applied to Hermitian or anti-Hermitian matrix arguments, and since the Fourier

extension approximates the identity map, the output is an accurate unitary block encoding of the non-unitary input. Since all linear operators can be decomposed into Hermitian and anti-Hermitian components, they can be expressed as a linear combination of unitaries with exponential convergence.

The Fourier-LCU method shifts from shrinking a convergence parameter used in existing methods,⁵ which simultaneously suppresses error and the usable signal as $\alpha = \text{poly}(1/\varepsilon)$, in favour of a global approximation strategy where the error and signal strength are only weakly coupled by $\alpha = O(\log \log[1/\varepsilon])$. This global basis provides a powerful framework for further customisations to meet the user's specific needs. The subnormalisation of the block encoding prepared by LCU is dependent on $S_m = \sum_{k=1}^m |a_k|$, and therefore penalises negative or imaginary coefficients. By exploiting the overcomplete nature of the Fourier extension, the user can explore a manifold of equivalent coefficient vectors to achieve the target error ε while minimising S_m (and hence α). The practical effect is counter-intuitive but robust; increasing the number of unitaries m can reduce subnormalisation, as the expanded expressivity of the basis provides more flexibility to lower α without sacrificing fidelity. In terms of asymptotic algorithmic advantage, the coefficients leading to exponential convergence are superior. But in practical quantum computing where producing high-quality block encodings is important, the regularised coefficients may be preferred.

The theoretical scaling arguments are supported by statevector simulations of a practical example, which show that a clear exponential convergence is obtained up to the double-precision floating-point accuracy. This result was obtained without excessively diminishing the usable signal, with a subnormalisation of up to $\alpha \approx 5$, thereby remaining within a regime that can feasibly be amplified. When the coefficients are instead selected via the regularised strategy, this improved to $\alpha \approx 2$, while still achieving a fidelity that is sufficient for the majority of applications.

In conclusion, Fourier LCU provides a broadly applicable route to constructing accurate, high-quality block encodings of non-unitary operators, without requiring specific structural symmetries or sparsity patterns, and thus may find broad application to quantum algorithm development. It may also serve as a robust access point to QSVT. Its end-to-end advantage is realised only when the required controlled implementations of $e^{\pm ik\tau H_1}$ and $e^{\pm ik\tau H_2}$ can be achieved at acceptable depth. In practice, this step is inherently problem-specific, so the main challenge in deploying Fourier LCU across many applications is identifying shallow circuit constructions for the underlying Hamiltonian simulations. This should then be integrated with an appropriate coefficient-selection strategy that accounts for the target application and the available hardware. These are the logical next steps towards turning the favourable scaling in m and α demonstrated here into useful quantum algorithms.

Acknowledgments

P. Brearley is supported by The University of Manchester via the Dame Kathleen Ollerenshaw Fellowship.

References

1. Childs, A. M. & Wiebe, N. Hamiltonian simulation using linear combinations of unitary operations. *Quantum Inf. & Comput.* **12**, 901–924 (2012).
2. Blanes, S., Casas, F. & Murua, A. Splitting methods for differential equations. *Acta Numer.* **33**, 1–161 (2024).
3. Childs, A. M., Kothari, R. & Somma, R. D. Quantum algorithm for systems of linear equations with exponentially improved dependence on precision. *SIAM J. on Comput.* **46**, 1920–1950 (2017).
4. Berry, D. W., Childs, A. M., Ostrander, A. & Wang, G. Quantum algorithm for linear differential equations with exponentially improved dependence on precision. *Commun. Math. Phys.* **356**, 1057–1081 (2017).
5. Schlimgen, A. W., Head-Marsden, K., Sager, L. M., Narang, P. & Mazzotti, D. A. Quantum simulation of open quantum systems using a unitary decomposition of operators. *Phys. Rev. Lett.* **127**, 270503 (2021).
6. Chowdhury, A. N. & Somma, R. D. Quantum algorithms for Gibbs sampling and hitting-time estimation. *Quantum Inf. & Comput.* **17**, 41–64 (2017).

7. Sanavio, C. & Succi, S. Lattice boltzmann–carleman quantum algorithm and circuit for fluid flows at moderate reynolds number. *AVS Quantum Sci.* **6** (2024).
8. Chakraborty, S., Morolia, A. & Peduri, A. Quantum regularized least squares. *Quantum* **7**, 988 (2023).
9. Gilyén, A., Su, Y., Low, G. H. & Wiebe, N. Quantum singular value transformation and beyond: exponential improvements for quantum matrix arithmetics. In *Proceedings of the 51st Annual ACM SIGACT Symposium on Theory of Computing*, 193–204 (2019).
10. Martyn, J. M., Rossi, Z. M., Tan, A. K. & Chuang, I. L. Grand unification of quantum algorithms. *PRX Quantum* **2**, 040203 (2021).
11. Koska, O., Baboulin, M. & Gazda, A. A tree-approach Pauli decomposition algorithm with application to quantum computing. In *ISC High Performance 2024 Research Paper Proceedings (39th International Conference)*, 1–11 (Prometeus GmbH, 2024).
12. Wan, L.-C. *et al.* Block-encoding-based quantum algorithm for linear systems with displacement structures. *Phys. Rev. A* **104**, 062414 (2021).
13. Over, P., Bengoechea, S., Brearley, P., Laizet, S. & Rung, T. Quantum algorithm for the advection-diffusion equation by direct block encoding of the time-marching operator. *Phys. Rev. A* **112**, L010401 (2025).
14. Wu, P. Additive combinations of special operators. *Banach Cent. Publ.* **30**, 337–361 (1994).
15. Li, X. *et al.* Toward quantum simulation of non-markovian open quantum dynamics: A universal and compact theory. *Phys. Rev. A* **110**, 032620 (2024).
16. Bharadwaj, S. S. & Sreenivasan, K. R. Compact quantum algorithms for time-dependent differential equations. *Phys. Rev. Res.* **7**, 023262 (2025).
17. Brassard, G., Hoyer, P., Mosca, M. & Tapp, A. Quantum amplitude amplification and estimation. *arXiv preprint quant-ph/0005055* (2000).
18. Fang, D., Lin, L. & Tong, Y. Time-marching based quantum solvers for time-dependent linear differential equations. *Quantum* **7**, 955 (2023).
19. Webb, M., Coppé, V. & Huybrechs, D. Pointwise and uniform convergence of fourier extensions. *Constr. approximation* **52**, 139–175 (2020).
20. Grover, L. K. A fast quantum mechanical algorithm for database search. In *Proceedings of the Twenty-Eighth Annual ACM Symposium on Theory of Computing*, 212–219 (1996).
21. Chen, S. S., Donoho, D. L. & Saunders, M. A. Atomic decomposition by basis pursuit. *SIAM review* **43**, 129–159 (2001).
22. Brent, R. P. An algorithm with guaranteed convergence for finding a zero of a function. *The computer journal* **14**, 422–425 (1971).
23. Barenco, A. *et al.* Elementary gates for quantum computation. *Phys. review A* **52**, 3457 (1995).
24. Low, G. H. & Chuang, I. L. Hamiltonian simulation by qubitization. *Quantum* **3**, 163 (2019).
25. Huybrechs, D. On the fourier extension of nonperiodic functions. *SIAM J. on Numer. Analysis* **47**, 4326–4355 (2010).

26. Berry, D. W., Childs, A. M., Cleve, R., Kothari, R. & Somma, R. D. Exponential improvement in precision for simulating sparse hamiltonians. In *Proceedings of the forty-sixth annual ACM symposium on Theory of computing*, 283–292 (2014).
27. Zecchi, A. A., Sanavio, C., Perotto, S. & Succi, S. Improved amplitude amplification strategies for the quantum simulation of classical transport problems. *Quantum Sci. Technol.* **10**, 035039 (2025).
28. Low, G. H. & Chuang, I. L. Optimal hamiltonian simulation by quantum signal processing. *Phys. review letters* **118**, 010501 (2017).
29. Hughes, A. *et al.* Trapped-ion two-qubit gates with > 99.99% fidelity without ground-state cooling. *arXiv preprint arXiv:2510.17286* (2025).

Table A. Fourier coefficients for exponential convergence in Eq. (6) for $m = 1, 2, 4, 8$, and 16 , using $\eta = 2 + 0.460m^{-0.319}$.

k	a_k	k	a_k
1	$1.1749265633763890 \times 10^0$	1	$1.9110596582766739 \times 10^0$
1	$1.4649300593981140 \times 10^0$	2	$-8.3329705463062109 \times 10^{-1}$
2	$-2.4671045529932240 \times 10^{-1}$	3	$4.4160671378740829 \times 10^{-1}$
1	$1.6867069657827318 \times 10^0$	4	$-2.3947858000595612 \times 10^{-1}$
2	$-4.9503423003210789 \times 10^{-1}$	5	$1.2560417538260940 \times 10^{-1}$
3	$1.2411979661060313 \times 10^{-1}$	6	$-6.1954442495961645 \times 10^{-2}$
4	$-1.7423091626316570 \times 10^{-2}$	7	$2.8214972876756641 \times 10^{-2}$
1	$1.8293489416481978 \times 10^0$	8	$-1.1685793781231944 \times 10^{-2}$
2	$-6.9782637202202591 \times 10^{-1}$	9	$4.3367104652322951 \times 10^{-3}$
3	$2.9318833555497786 \times 10^{-1}$	10	$-1.4182928702138838 \times 10^{-3}$
4	$-1.1239628137353329 \times 10^{-1}$	11	$4.0046998527214087 \times 10^{-4}$
5	$3.6120497884196093 \times 10^{-2}$	12	$-9.4993240608959911 \times 10^{-5}$
6	$-8.9919401310510454 \times 10^{-3}$	13	$1.8196971126400890 \times 10^{-5}$
7	$1.5370025210256612 \times 10^{-3}$	14	$-2.6440238988517658 \times 10^{-6}$
8	$-1.3579108324114441 \times 10^{-4}$	15	$2.5962936805754857 \times 10^{-7}$
		16	$-1.2959054619319566 \times 10^{-8}$

Table B. Fourier coefficients for Eq. (6) to minimise the LCU subnormalisation α defined in Eq. (14) for the optimal path $\lambda \rightarrow 0$, with $m = 8, 16, 32$ and 64 terms and using $\eta = 2 + 0.460m^{-0.319}$.

k	a_k
1	$1.6252703132458948 \times 10^0$
2	$-3.8683393390100113 \times 10^{-1}$
3	$2.9701926916938142 \times 10^{-6}$
4	$8.6366199973602994 \times 10^{-2}$
5	$-6.2709967227889740 \times 10^{-2}$
6	$2.5797568201661875 \times 10^{-2}$
7	$-6.2821777289429268 \times 10^{-3}$
8	$7.0516066255388169 \times 10^{-4}$

k	a_k	k	a_k
1	$1.2916284406688450 \times 10^0$	1	$1.2724940501206685 \times 10^0$
2	$-8.2928182586576808 \times 10^{-6}$	2	$1.7647437339825657 \times 10^{-4}$
3	$-1.6380870072858236 \times 10^{-1}$	3	$-1.4029956194722445 \times 10^{-1}$
4	$-1.1749055646727718 \times 10^{-4}$	4	$-1.7466439143801946 \times 10^{-3}$
5	$9.5121401363295541 \times 10^{-2}$	5	$5.1972157370992783 \times 10^{-2}$
6	$-4.4101764557668302 \times 10^{-2}$	6	$-1.2950516021742702 \times 10^{-5}$
7	$-3.0991164009267009 \times 10^{-2}$	7	$-2.6250415571873853 \times 10^{-2}$
8	$3.7272526527023730 \times 10^{-2}$	8	$-2.0045263795425770 \times 10^{-4}$
9	$1.1172975770566466 \times 10^{-9}$	9	$1.6194718073768280 \times 10^{-2}$
10	$-1.7158480316302412 \times 10^{-2}$	10	$-1.7795597389026188 \times 10^{-5}$
11	$1.0227568020830558 \times 10^{-6}$	11	$-1.0947086763603864 \times 10^{-2}$
12	$2.1591424416141321 \times 10^{-2}$	12	$-1.613055334899803 \times 10^{-5}$
13	$-2.5086222729521594 \times 10^{-2}$	13	$8.1213598893640250 \times 10^{-3}$
14	$1.5028650505911973 \times 10^{-2}$	14	$-1.0105205711471294 \times 10^{-5}$
15	$-5.1021757768611713 \times 10^{-3}$	15	$-6.5220377643697468 \times 10^{-3}$
16	$8.0061388231784947 \times 10^{-4}$	16	$1.4019018381270808 \times 10^{-4}$

k	a_k	k	a_k	k	a_k
1	$1.2674734015491065 \times 10^0$	23	$-7.9463150834943651 \times 10^{-4}$	45	$1.0067897136897290 \times 10^{-3}$
2	$1.7244036026329542 \times 10^{-3}$	24	$-1.6106715619342506 \times 10^{-3}$	46	$5.9588480131204046 \times 10^{-4}$
3	$-1.3651956841899426 \times 10^{-1}$	25	$-4.9464035326807751 \times 10^{-6}$	47	$-6.5786065655079997 \times 10^{-4}$
4	$-3.7491316708631625 \times 10^{-3}$	26	$2.3220958796745187 \times 10^{-3}$	48	$-7.9071836196200783 \times 10^{-4}$
5	$4.9938995414798140 \times 10^{-2}$	27	$-7.8337502650478882 \times 10^{-4}$	49	$1.0383768769934927 \times 10^{-3}$
6	$2.0537857315178420 \times 10^{-5}$	28	$-1.4467190801562466 \times 10^{-3}$	50	$3.2379462694742472 \times 10^{-4}$
7	$-2.2365029891127992 \times 10^{-2}$	29	$5.9948907915225263 \times 10^{-5}$	51	$-8.9639232053924400 \times 10^{-4}$
8	$-2.1986888801476118 \times 10^{-3}$	30	$1.9888623342606952 \times 10^{-3}$	52	$-1.3614874919487633 \times 10^{-4}$
9	$1.4415085643057280 \times 10^{-2}$	31	$-6.1980733169232454 \times 10^{-4}$	53	$7.6632791961643262 \times 10^{-4}$
10	$-3.0068477747746482 \times 10^{-5}$	32	$-1.4466978071478636 \times 10^{-3}$	54	$1.7582497598172885 \times 10^{-4}$
11	$-7.4716874776132548 \times 10^{-3}$	33	$3.1933413688348182 \times 10^{-4}$	55	$-1.1303466077145865 \times 10^{-3}$
12	$-1.2580044370038269 \times 10^{-3}$	34	$1.5499247480596221 \times 10^{-3}$	56	$5.5314082202381201 \times 10^{-4}$
13	$5.5788601054847075 \times 10^{-3}$	35	$-4.4182222940644011 \times 10^{-4}$	57	$6.8367594233895623 \times 10^{-4}$
14	$2.1058401322186844 \times 10^{-4}$	36	$-1.4707022815413659 \times 10^{-3}$	58	$-8.4905815050110005 \times 10^{-4}$
15	$-2.8383216657104390 \times 10^{-3}$	37	$6.1240547093369786 \times 10^{-4}$	59	$-1.5612025010239042 \times 10^{-4}$
16	$-5.3130644207911078 \times 10^{-4}$	38	$1.1440602210948403 \times 10^{-3}$	60	$1.0500974069199117 \times 10^{-3}$
17	$1.1591597789557177 \times 10^{-3}$	39	$-3.5492407433698856 \times 10^{-4}$	61	$-1.0642102482310875 \times 10^{-3}$
18	$1.2506220453015711 \times 10^{-3}$	40	$-1.4202668982435333 \times 10^{-3}$	62	$5.6268780177663074 \times 10^{-4}$
19	$-4.6549080425110673 \times 10^{-4}$	41	$8.5303847289379061 \times 10^{-4}$	63	$-1.5878937168396719 \times 10^{-4}$
20	$-1.7343772935326910 \times 10^{-3}$	42	$8.3460819270331189 \times 10^{-4}$	64	$1.7297084483843702 \times 10^{-5}$
21	$9.2174698931998786 \times 10^{-5}$	43	$-4.2780663107703745 \times 10^{-4}$		
22	$2.4160104742981634 \times 10^{-3}$	44	$-1.2161903222093979 \times 10^{-3}$		